

ARTICLES

Solvothermal Synthesis of Monodisperse PbSe Nanocrystals

Jian Xu, Jian-Ping Ge, and Ya-Dong Li*

Department of Chemistry, Tsinghua University, Beijing 100084, People's Republic of China

Received: November 10, 2005; In Final Form: December 21, 2005

Size-controllable monodisperse PbSe and PbSe/PbS nanocrystals (NCs) have been successfully synthesized with a solvothermal method. Octadecylamine (ODA) molecules were found effective in organizing the nanocrystals to form an ordered monolayer. It is expected that these narrow-band-gap semiconductor NCs with tunable size would have potential applications in near- and mid-IR telecommunication laser sources, electroluminescence, and solar cell materials.

Over the past decade colloidal nanocrystals (NCs) which are monodisperse in size and shape have received substantial attention due to their unique optical and physical properties compared to bulk materials.^{1–7} However, it is still a great challenge to prepare narrow-size-distribution nanocrystals. In the present work, we use a solvothermal method to prepare a high-quality ODA-capped PbSe nanocrystal, an important narrow-band-gap IV–VI group semiconductor, which is highly desirable in potential applications such as near-IR light sources and lasers,^{8,9} nonlinear optical switches,¹⁰ biomedical imaging and labeling,¹¹ solar cell sensitizers,^{12,13} and size-tunable narrow-bandwidth photoluminescence (PL) emissions.^{14–15}

Various approaches are explored to pursue a simple and size-tunable synthetic route for IV–VI semiconductor monodisperse NCs, including polymer and glass matrix host methods^{16,17} and gas-phase,^{18,19} solid-state,²⁰ and solution-phase syntheses.^{21,22} Among these methods, it is well-established that synthetic routes utilizing organometallic/nonmetallic precursors enable production of high-quality monodisperse semiconductors, metals, and metal oxide NC dispersions. Since the first synthesis for monodisperse PbSe colloidal NCs using trioctylphosphine (TOP) selenide precursors in trioctylphosphine by Murray et al.,²³ some similar approaches in solution phase have been reported.^{24–28} On the other hand, several reports utilized single organometallic molecular precursors such as lead–cyclohexanecarboxylate or Pb(S₂CNEt₂)₂ to obtain PbSe or PbS NCs.^{29,30} Moreover, Hyeon's group utilized a facile coordinating solvent route to obtain uniform cube-shaped PbS NCs with particle sizes of 6, 8, 9, and 13 nm.³¹ However, few efforts are devoted to synthesizing PbSe monodisperse NCs using a simple and nontoxic solution route without tedious size-selection processes and expensive organometallic/nonmetallic precursors.

Recently, our group has established a facile solvothermal approach to obtain II–VI group semiconductor nanorods or nanocrystals including CdE (E = S, Se, Te) and ZnE (E = S, Se).³² Short-chain alkylamines such as ethylenediamine were used as structure-directing coordination molecular templates, which have been proven responsible for the morphologies and

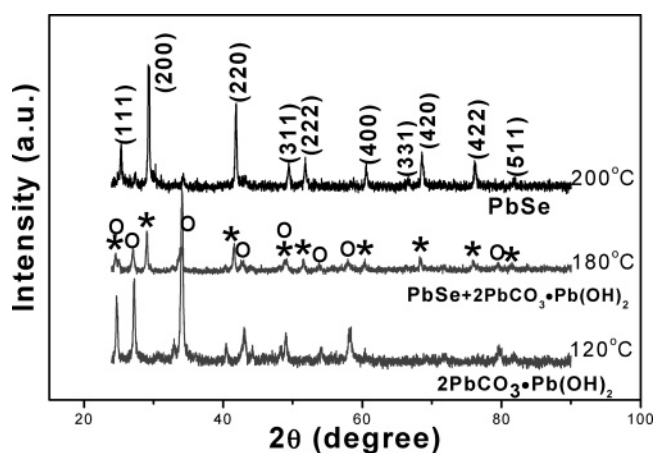


Figure 1. XRD patterns for PbSe NCs prepared at different temperatures as indicated. An asterisk refers to cubic phase PbSe, and circle mark is for hexagonal phase 2PbCO₃·Pb(OH)₂.

sizes of products. This traditional solvothermal method was further developed in this work with the introduction of long-chain alkylamines, which is conducted simply by the reaction of lead acetate and Se powder in nontoxic octadecylamine, and no further size-selection processes are required. Due to the special reactivity under high temperature and high pressure, Se powder can be directly used as Se sources, which avoids usage of its toxic precursors. Furthermore, the as-obtained PbSe NCs could be easily transferred to nearly monodisperse PbSe/PbS core/shell nanostructures by capping of PbS at mild conditions.

In a typical synthesis of 16 nm PbSe monodisperse NCs, Pb(CH₃COO)₂·3H₂O (2 mmol) was dissolved in octadecylamine (20 mL) to form a clear solution under heating and stirring, which was kept at 80 °C for ~4 h. A 1 mmol amount of Se powder was added rapidly into the solution and stirred vigorously for ~10 min. Then the resulting mixture was sealed in a Teflon-lined stainless steel autoclave and maintained at 200 °C for 1.5 h. After the solution was allowed to cool to room temperature, the gray precipitates were washed several times with anhydrous ethanol and dried at 60 °C for 4 h. Adjusting the molar ratio of initial Pb²⁺:Se from 1:0.33, 1:0.5, 1:0.7, to

* To whom correspondence should be addressed. E-mail: ydli@mail.tsinghua.edu.cn.

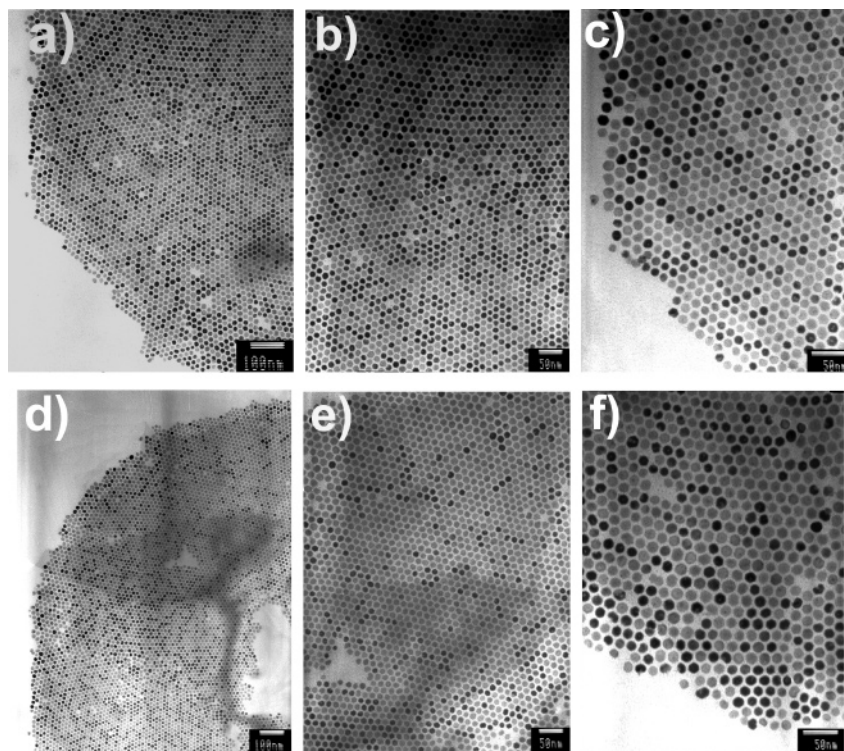


Figure 2. TEM images with different magnifications for 13 nm PbSe NCs (a–c) and 16 nm PbSe NCs (d–f), respectively.

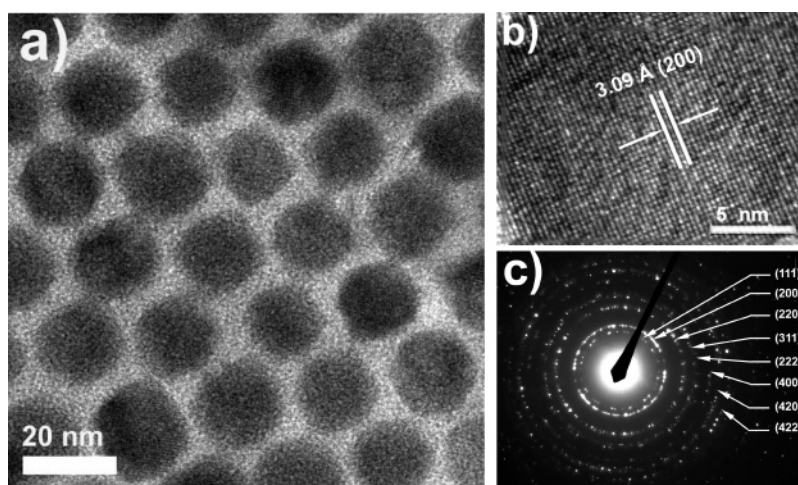


Figure 3. (a) Low-resolution TEM image for 16 nm PbSe NCs; (b) HRTEM lattice image for a single NC; (c) SAED pattern for NCs shown in a.

1:1, the nanocrystals with sizes of 11, 16, 19, 50 nm could be selectively prepared.

To prepare PbSe/PbS core/shell NCs, some treatments were taken just after the cooling of the products in the autoclave. S powder or thioacetamide was directly added to the as-prepared PbSe NCs in the original octadecylamine solution to maintain a constant S:Se molar ratio of 1:1. Then the mixture was sealed again in a Teflon-lined stainless steel autoclave and heated at 80 °C for 4 h. The color of the final solution changed to deep-gray, implying the formation of the PbS shell. The precipitates were washed and dried following procedure similar to that mentioned above.

The phase purities of all the obtained samples were measured on a Bruker D8-advance X-ray powder diffractometer with Cu K α radiation ($\lambda = 1.5418$ Å). A small amount of products was dispersed in ethanol by ultrasonic treatment for ~ 10 min. Then one drop of the resulting solution was placed onto a carbon-

coated copper grid and dried at room temperature for next TEM (transmission electron microscope) and HRTEM (high-resolution transmission electron microscope) visualization. The lower resolution TEM images were recorded by a JEM 1200EX transmission electron microscope, and HRTEM lattice images and SAED (selected-area electron diffraction), together with EDS (electron dispersive spectrum), were obtained on a JEOL JEM-2010F high-resolution transmission electron microscope.

The crystalline structures of PbSe were characterized by X-ray diffraction (XRD) analysis. As shown in Figure 1 (top pattern), all diffraction peaks can be easily indexed to the cubic rock salt PbSe phase (JCPDS 78-1903). The reaction temperature is found to be important to ensure the yield of pure-phase cubic PbSe NCs. As testified by X-ray diffraction (XRD) patterns, products obtained above 200 °C are pure cubic phase PbSe, whereas those obtained at 180 °C are mixtures of PbSe and $2\text{PbCO}_3 \cdot \text{Pb}(\text{OH})_2$, and only $2\text{PbCO}_3 \cdot \text{Pb}(\text{OH})_2$ yields at 120 °C.

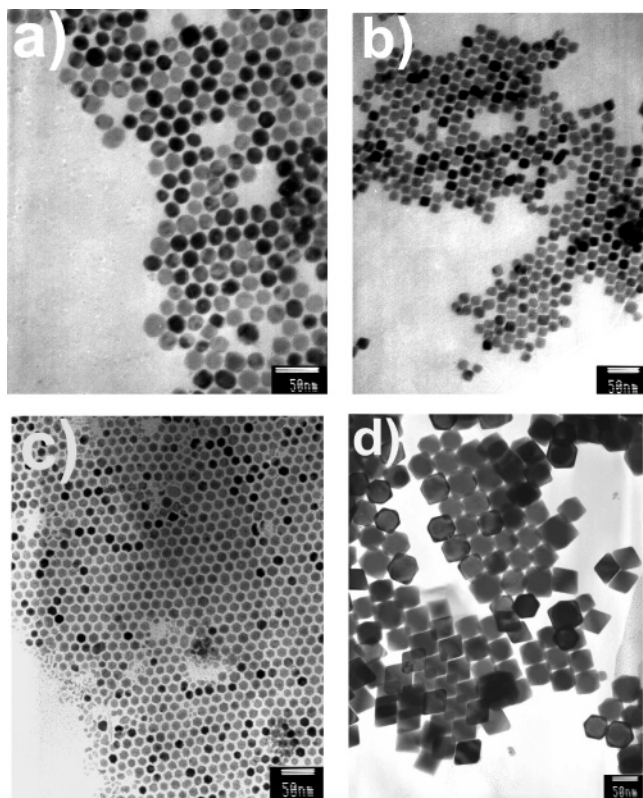


Figure 4. TEM images for PbSe NCs with different sizes and shapes: (a) 19 nm spherical; (b) 19 nm cubic; (c) 13 nm hexagonal; and (d) 50 nm polyhedral shape.

Since the decomposition temperature of reactant $\text{Pb}(\text{CH}_3\text{COO})_2 \cdot 3\text{H}_2\text{O}$ is just above 200 °C,^{33,34} it is reasonable to deduce that this unique thermodecomposition process may improve the reactivity of the lead source with the Se powder to enable the formation of monodisperse PbSe NCs. The melting of Se powder has little effect on the formation of cubic phase PbSe, because it begins to form at 180 °C, which is far below its melting point (221 °C).

The size and shape monodispersities of products were examined by TEM imaging. Figure 2 shows typical images of 13 and 16 nm PbSe NCs, which have spherical morphologies and very narrow particle diameter distributions. The standard deviations of size distributions are estimated as ~ 5.5 and $\sim 5.0\%$ for 13 and 16 nm NCs, respectively. The diameter distribution histograms of them are shown in Figure S1 (see Supporting Information).

HRTEM analysis provides more insights into the crystal structures of these NCs. A representative low-resolution TEM image for 16 nm PbSe NCs (Figure 3a) shows an ordered two-dimensional arrangement attributed to the high monodispersity. As shown in Figure 3b, the HRTEM lattice fringes image reveals the single-crystalline nature of as-obtained NCs without detectable stacking faults or crystal defects. The lattice spacing is calculated as ~ 3.09 Å, which is consistent with the interlayer separation between (200) lattice planes for bulk PbSe (JCPDS 78-1903, $d_{200} = 3.06$ Å). Furthermore, SAED patterns (Figure 3c) index well to cubic rock salt PbSe crystal structure and also confirm the strongest diffraction ring as (200) planes.

In the present work, the molar ratio of initial reactants is found to be crucial in determining the size and shape of the final products, although the size is generally influenced by the reaction time and the concentration of the starting material. As shown in Figures 2 and 4, at the constant lead acetate concentration and temperature (e.g., 0.1 M, 200 °C), the sizes

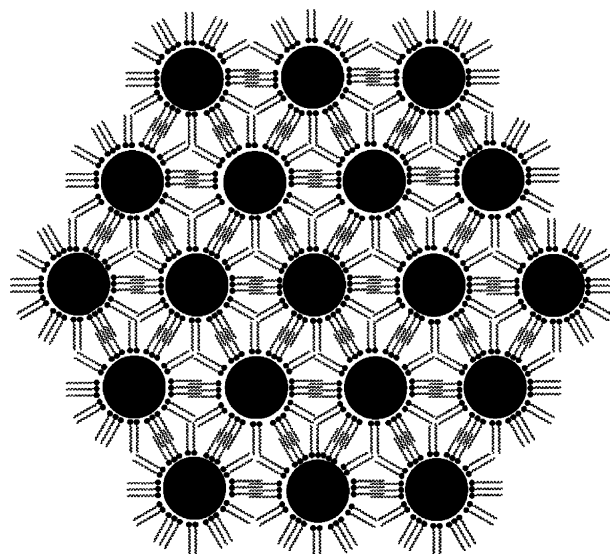


Figure 5. Self-assembly of spherical 16 nm PbSe nanocrystal monolayer in hexagonal close packing.

of the NCs vary from 13, 16, 19 to 50 nm when the initial molar ratio of $\text{Pb}^{2+}:\text{Se}$ is changed from 1:0.33, 1:0.5, 1:0.7 to 1:1, respectively. However, changing either the reaction time or the absolute reactant concentrations, due to the complicated nucleation and growth process, shows no straightforward correlation between them and the size or shape.

A distinctive shape transition from spherical- to cubic-shaped NCs is observed with increasing size (see Figures 2 and 4). At relatively small sizes (<19 nm in this work), it is well-recognized that PbSe NCs are spherical in shape.²⁷ It is because small spherelike particles are the lowest energy form that have the minimum surface-to-volume ratio; namely, the surface energy contributions are dominant in defining a hexagonal close packing pattern. With size increases, the intrinsic crystal structure becomes the dominating contributions; thus, the cubic rock salt PbSe NCs tend to arrange in a cubic shape for larger particles. For 19 nm NCs, the coexistence of both spherical and cubic shapes on the same TEM grid implies that such shape transition occurs during the growth process. Finally, when the size exceeds 50 nm ($\text{Pb}^{2+}:\text{Se} = 1:1$), most of the NCs are cubiclike, which tend to aggregate to some extent.

In our synthesis, ODA plays two important roles. First, it is an effective stabilizer which limits the crystal growth at high temperature and direct forming high-quality monodisperse PbSe nanocrystals. The N atom of the ODA molecule has strong coordination ability, which could easily stick to the surface of many inorganic nanocrystals, just like oxygen and phosphor ligands. Second, ODA acts as a soft template that directs the NCs to form a monolayer on the amorphous carbon film of a copper grid. Taking the 16 nm PbSe nanocrystals as an instance, the intermolecular van der Waals force attracts the neighboring particles together to form a hexagonal close packing superstructure due to their spherical shape (Figure 5). HRTEM observation shows the distance between two neighboring particles was 3.37 nm on average. The ODA molecule was estimated to be about 2.26 nm in length according to the C—C bond length and geometrically straight-line conformation. Therefore, it is interesting to know that half of the ODA chains in length overlap. They do not overlap completely maybe because of the steric hindrance of the ODA molecules.

Since the combination of two inorganic materials with different band gaps is expected to achieve an energy tuning of the exciton transitions between them,³⁵ nearly monodisperse

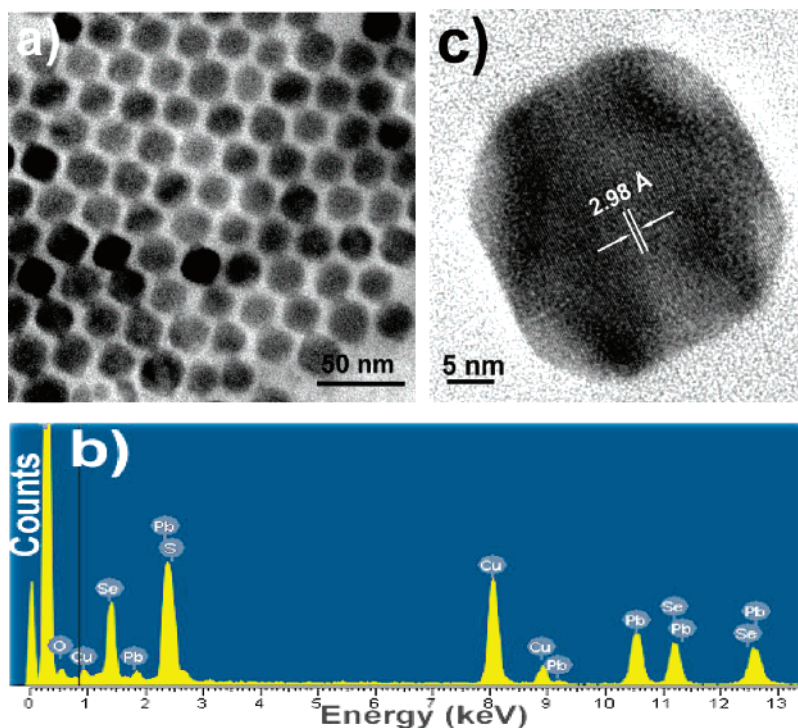


Figure 6. (a) Low-resolution TEM image for 20 nm PbSe/PbS core/shell NCs; (b) EDS spectrum for NCs shown in a; (c) HRTEM lattice image for single truncated cubelike NC.

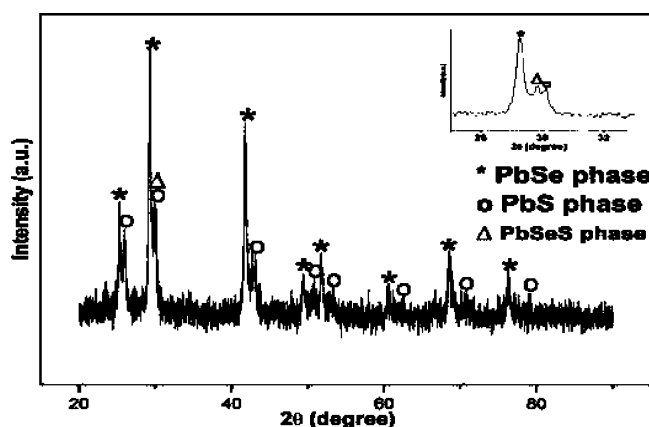


Figure 7. XRD pattern for ~20 nm PbSe/PbS core/shell NCs prepared using S powder as the S source. The NCs consist of cubic phase PbSe and PbS, together with a new peak as shown in the inset assumed to be the $\text{PbSe}_x\text{S}_{1-x}$ solid solution phase.

PbSe/PbS core/shell NCs were prepared through capping of the in situ generated 16 nm PbSe NCs. In the previous step to produce 16 nm PbSe, the $\text{Pb}^{2+}:\text{Se}$ molar ratio is 1:0.5. So the excess Pb^{2+} in situ will react with additional S to form PbS. TEM images show the samples are pure 20 nm nanocrystals, and EDS analysis proved every single particle is composed of Se and S (Figure 6). It should be noted again that PbSe would not decompose or grow up by prolonging the reaction time, while the corresponding XRD pattern actually consists of both PbS and PbSe phases (Figure 7). Therefore, the PbSe-core/PbS-shell structure will be the most reasonable speculation we can conclude. HRTEM image shows no clear boundary at the core/shell interface maybe because of the close lattice matching between PbSe and PbS. The lattice spacing is examined as about 2.98 Å, which falls between that of bulk PbSe (JCPDS 78-1903, $d_{200} = 3.06$ Å) and PbS (JCPDS 78-1899, $d_{200} = 2.96$ Å).

In contrast, by choosing thioacetamide as the S source at the same reaction conditions, starlike PbSe/PbS core/shell nano-

particles with sizes located within 30–120 nm were obtained (see Figure S2 in Supporting Information). It is possibly because the thioacetamide is more reactive than the S powder, resulting in larger size particles in relatively disordered arrangement.

In conclusion, size-controllable monodisperse PbSe and PbSe/PbS NCs have been successfully synthesized with a solvothermal method. Instead of using expensive and toxic organometallic/nonmetallic precursors and a tedious size-selection process, the simple reaction between Se powders and lead acetate in nontoxic solvent suggests a safe and cheap route for scaled-up production of monodisperse NCs. It is expected that these narrow-band-gap semiconductor NCs with tunable size would have potential applications in near- and mid-IR telecommunication, laser sources, electroluminescence devices, and Gratzel solar cells.

Acknowledgment. This work was supported by NSFC Grant 90406003 and the State Key Project of Fundamental Research for Nanomaterials and Nanostructures (Grant 2003CB716901).

Supporting Information Available: Figures showing particle size distribution histograms of spherical PbSe NCs and HREM images for PbSe/PbS core/shell NCs. This material is available free of charge via the Internet at <http://pubs.acs.org>.

References and Notes

- (1) (a) Huynh, W.; Peng, X.; Alivisatos, A. P. *Adv. Mater.* **1999**, *11*, 923. (b) Peng, X.; Schlamp, M. C.; Kadavanich, A. V.; Alivisatos, A. P. *J. Am. Chem. Soc.* **1997**, *119*, 7019. (c) Peng, X.; Manna, L.; Yang, W.; Wickham, J.; Scher, E. C.; Kadavanich, A.; Alivisatos, A. P. *Nature* **2000**, *404*, 59.
- (2) (a) Murray, C. B.; Norris, D. J.; Bawendi, M. G. *J. Am. Chem. Soc.* **1993**, *115*, 8706. (b) Murray, C. B.; Kagan, C. R.; Bawendi, M. G. *Annu. Rev. Mater. Sci.* **2000**, *30*, 8706.
- (3) (a) Trentler, T. J.; Hickman, K. M.; Goel, S. C.; Viano, A. M.; Gibbons, P. C.; Buhro, W. E. *Science* **1995**, *270*, 1791. (b) Yu, H.; Li, J. B.; Loomis, R. A.; Wang, L. W.; Buhro, W. E. *Nat. Mater.* **2003**, *2*, 517.
- (4) (a) Hazarika, P.; Ceyhan, B.; Niemeyer, C. M. *Angew. Chem., Int. Ed.* **2004**, *43*, 6469. (b) Dumestre, F.; Chaudret, B.; Amiens, C.; Respaud, M.; Fejes, P.; Renaud, P.; Zurcher, P. *Angew. Chem., Int. Ed.* **2003**, *42*, 5213.

- (5) (a) Zoldesi, C. I.; Imhof, A. *Adv. Mater.* **2005**, *17*, 924. (b) Kudara, S.; Carbone, L.; Casula, M. F.; Cingolani, R.; Falqui, A.; Snoeck, E.; Parak, W. J.; Manna, L. *Nano Lett.* **2005**, *5*, 445.
- (6) (a) Seo, W. S.; Jo, H. H.; Lee, K.; Kim, K. B.; Oh, S. J.; Park, J. T. *Angew. Chem., Int. Ed.* **2004**, *43*, 1115. (b) Park, J.; Kang, E.; Son, S. U.; Park, H. M.; Lee, M. K.; Kim, J.; Kim, K. W.; Noh, H. J.; Park, J. H.; Bae, C. J.; Park, J. G.; Hyeon, T. *Adv. Mater.* **2005**, *17*, 429.
- (7) (a) Sun, S. H.; Zeng, H.; Robinson, D. B.; Raoux, S.; Rice, P. M.; Wang, S. X.; Li, G. X. *J. Am. Chem. Soc.* **2004**, *126*, 273. (b) Sun, S. H.; Anders, S.; Thomson, T.; Baglin, J. E.; Toney, M. F.; Hamann, H. F.; Murray, C. B.; Terris, B. D. *J. Phys. Chem. B* **2003**, *107*, 5419.
- (8) Xu, H. Z.; Zhao, F.; Majumdar, A.; Jayasinghe, L.; Shi, Z. *Electron. Lett.* **2003**, *39*, 659.
- (9) Sirota, M.; Galun, E.; Krupkin, V.; Glushko, A.; Kigel, A.; Brumer, M.; Sashchiuk, A.; Amirav, L.; Lifshitz, E. *Proc. SPIE-Int. Soc. Opt. Eng.* **2004**, *9*, 5510.
- (10) Wise, F. W. *Acc. Chem. Res.* **2000**, *33*, 773.
- (11) Lim, Y. T.; Kim, S.; Nakayama, A.; Stott, N. E.; Bawendi, M. G.; Frangioni, J. V. *Mol. Imaging* **2003**, *2*, 50.
- (12) Plass, R.; Pelet, S.; Krueger, J.; Gratzel, M.; Bach, U. *J. Phys. Chem. B* **2002**, *106*, 7578.
- (13) Schaller, R. D.; Klimov, V. I. *Phys. Rev. Lett.* **2004**, *92*, 186601.
- (14) Hines, M. A.; Scholes, G. D. *Adv. Mater.* **2003**, *15*, 1844.
- (15) Sargent, E. H. *Adv. Mater.* **2005**, *17*, 515.
- (16) Wang, S. H.; Yang, S. H. *Langmuir* **2000**, *16*, 389.
- (17) Lipovskii, A.; Kolobkova, E.; Petrikov, V.; Kang, I.; Olkhovets, A.; Krauss, T.; Thomas, M.; Silcox, J.; Wise, F.; Shen, Q.; Kycia, S. *Appl. Phys. Lett.* **1997**, *71*, 3406.
- (18) Kaito, C.; Saito, Y.; Fujita, K. *Jpn. J. Appl. Phys.* **1987**, *26*, 1973.
- (19) Ge, J. P.; Wang, J.; Zhang, H. X.; Wang, X.; Peng, Q.; Li, Y. D. *Chem. Eur. J.* **2005**, *11*, 1889.
- (20) Wang, W.; Liu, Y.; Zhan, Y.; Zheng, C.; Wang, G. *Mater. Res. Bull.* **2001**, *36*, 1977.
- (21) Nenadovice, M. T.; Comor, M. I.; Vasic, V.; Micic, O. I. *J. Phys. Chem.* **1990**, *94*, 6390.
- (22) Wang, C.; Zhang, G.; Fan, S. S.; Li, Y. D. *J. Phys. Chem. Solids* **2001**, *62*, 1957.
- (23) Murray, C. B.; Sun, S.; Gaschler, W.; Doyle, H.; Betley, T. A.; Kagan, C. R. *IBM J. Res. Dev.* **2001**, *45*, 47.
- (24) Wehrenberg, B. L.; Wang, C.; Guyot-Sionnest, P. *J. Phys. Chem. B* **2002**, *106*, 10634.
- (25) Du, H.; Chen, C.; Krishnan, R.; Krauss, T. D.; Harbold, J. M.; Wise, F. W.; Thomas, G. J. *Nano Lett.* **2002**, *2*, 1321.
- (26) Yu, W. W.; Falkner, J. C.; Shih, B. S.; Colvin, V. L. *Chem. Mater.* **2004**, *16*, 3318.
- (27) Petryga, J. M.; Schaller, R. D.; Werder, D.; Stewan, M. H.; Klimov, V. I.; Hollingsworth, J. A. *J. Am. Chem. Soc.* **2004**, *126*, 11752.
- (28) (a) Sashchiuk, A.; Langof, L.; Chaim, R.; Lifshitz, E. *J. Cryst. Growth* **2002**, *240*, 431. (b) Lifshitz, E.; Bashouti, M.; Kloper, V.; Kigel, A.; Eisen, M. S.; Berger, S. *Nano Lett.* **2003**, *3*, 857. (c) Sashchiuk, A.; Amirav, L.; Bashouti, M.; Krueger, M.; Sivan, U.; Lifshitz, E. *Nano Lett.* **2003**, *3*, 159.
- (29) Sashchiuk, A.; Amirav, L.; Bashouti, M.; Krueger, M.; Sivan, U.; Lifshitz, E. *Nano Lett.* **2004**, *4*, 159.
- (30) Lee, S. M.; Jun, Y. W.; Cho, S. N.; Cheon, J. *J. Am. Chem. Soc.* **2002**, *124*, 11244.
- (31) Joo, J.; Na, H. B.; Yu, T.; Yu, J. H.; Kim, Y. W.; Wu, F. X.; Zhang, J. Z.; Hyeon, T. *J. Am. Chem. Soc.* **2003**, *125*, 11100.
- (32) (a) Li, Y. D.; Ding, Y.; Qian, Y. T.; Zhang, Y.; Yang, L. *Inorg. Chem.* **1998**, *37*, 2844. (b) Li, Y. D.; Liao, H. W.; Ding, Y.; Qian, Y. T.; Yang, L.; Zhou, G. E. *Chem. Mater.* **1998**, *10*, 2301. (c) Li, Y. D.; Liao, H. W.; Ding, Y.; Fan, Y.; Zhang, Y.; Qian, Y. T. *Inorg. Chem.* **1999**, *38*, 1382. (d) Deng, Z. X.; Wang, C.; Sun, X. M.; Li, Y. D. *Inorg. Chem.* **2002**, *41*, 869. (e) Deng, Z. X.; Li, L. B.; Li, Y. D. *Inorg. Chem.* **2003**, *42*, 2331.
- (33) Leibold, R.; Huber, F. *J. Therm. Anal.* **1980**, *18*, 493.
- (34) Xu, J.; Li, Y. D. *Chem. J. Chin. Univ.* **2004**, *25*, 595.
- (35) Brumer, M.; Kigel, A.; Amirav, L.; Sashchiuk, A.; Solomesch, O.; Tessler, N.; Lifshitz, E. *Adv. Funct. Mater.* **2005**, *15*, 1111.